# Coarse-Grain Simulations of Solid Supported Lipid Bilayers with Varying Hydration Levels

Florian Benedetti, Li Fu, Fabrice Thalmann, Thierry Charitat, Anne Rubin, Claire Loison

# Coarse-Grain Simulations of Solid Supported Lipid Bilayers with Varying Hydration Level

Florian Benedetti,[†,¶] Li Fu,[‡,§] Fabrice Thalmann,[‡] Thierry Charitat,[‡] Anne Rubin,[‡] and Claire Loison[*,†]

†*University of Lyon, Université Claude Bernard Lyon 1, CNRS, Institut Lumière Matière, F-69622, Villeurbanne, France*

‡*Institut Charles Sadron, Université de Strasbourg, CNRS, 23 rue du Loess, BP 84047 67034 Strasbourg Cedex 2, France*

¶*Current address: Institut für Theoretische Physik, Technische Universitat Wien, Vienna, Austria*

§*Current address: Univ Lyon, Ecole Centrale de Lyon, Laboratoire de Tribologie et Dynamique des Systèmes, UMR 5513, 36 avenue Guy de Collongue, 69134 Ecully Cedex, France*

E-mail: claire.loison@univ-lyon1.fr

**Abstract**

Supported lipid bilayers (SLBs) are a very popular system for the study of biomimetic membranes. Understanding of the interactions between the solid substrate and the lipid membrane opens pathways to the design of new materials with fine-tunable properties. While it is possible to study SLBs via Molecular Dynamics (MD) simulations, difficulties still remain for these strategies; in particular, the confined water layer thickness and structure are difficult to reproduce in simulations. We have explored different coarse-grained (CG) models for the membrane/support interaction, and their impact on the substrate hydration level. Our results highlight the relevance of including long-range interactions in CG-MD simulations of fluid SLBs. Modeled neutron reflectivity curves are deduced from the structures obtained by molecular simulations, and substrate parameters are optimized to match the experimental and modeled reflectivity curves. We expect our coarse-grained approach to open new perspectives for the simulations of SLBs of increasing complexity, including lipid layers of complex compositions, or adsorbed lipidic layers on patterned surfaces.

# 1 Introduction

Model lipid membranes are widely used to study biological processes that take place in the plasma membrane and inner-cellular compartments[1]. Solid-supported lipid bilayers (SLBs), as a popular cell membrane mimic, show complementary advantages relative to Langmuir monolayers, unilamellar or multillamelar vesicles[1]. SLBs are also used for their numerous applications in food industry, bionanotechnologies, and material design[2,3].

The understanding of the influence of the preparation method, and of the interaction with each solid substrate is crucial to fully exploit these model systems. In particular, it permits to design new materials which properties are fine-tuned based on the membrane/support interactions[3,4].

The SLBs' stability and their constrained orientation make it possible to study them using

surface-sensitive measurement techniques such as atomic force microscopy, particle tracking via fluorescence measurements, surface plasmon resonance, surface second harmonic generation spectrometry, neutron or X-ray specular reflectometry[5–10]. Molecular dynamics (MD) simulations can also be advantageously used to investigate SLBs, to cross-validate the results of the experimental approaches, or to provide structural and dynamical descriptions at the molecular level[5,11? –15]. Despite the molecular insight that can be gained by numerical simulations[13,16–20], relatively few computational studies have been reported yet (see the review by Hirtz et al.[21]). Indeed, both experiments and simulations[8,22–24] have highlighted how strongly the SLB properties change, depending on the interplay between the membrane/solid, membrane/solvent and solid/solvent interactions.

In particular, the hydration level and the substrate surface are important factors affecting lipid organization. The effects of the substrate inhomogeneities or rugosity at nanometer scale are more easily represented using coarse-grained models[17,25,26], but direct comparisons with experimental data at the molecular scale remain difficult. On the opposite, all-atoms models describe more precisely the confined hydration water[27], but simulations dealing with the substrate complexity[?] remain scarce because of computational costs. The "semi-quantitative" model Martini[28,29] is a promising level of coarse-graining to study complex SLBs structures while keeping enough molecular details to compare to experimental data, at least for some phosphocholine lipids[13,30]. It is very popular for lipid bilayer and monolayer simulations[31], and was exploited to simulate supported bilayers with results showing structural and dynamical differences between the two monolayers of a SLB, and the importance of long-range interactions[13,16,18,19,22,32].

One of the difficulties encountered in SLB simulations using Martini models is the high crystallization temperature of the CG-water ($290 \pm 5$ K[16,29]). Nearby a support, it may even crystallize at temperature as high as 323 K[33]. Anti-freeze water particles, or Martini polarized water model[34] did not impede completely crystallization near a planar wall[32,35]. To avoid unphysical crystallization nearby the support, a "weak water model" was pro-

posed[33], in which the water/water Lennard-Jones (LJ) interactions are attenuated. This weak water model gained in popularity for SLB simulations[16,18,19,32,36], but Lamberg et al. recently demonstrated that this weak water/water interaction indirectly changes the solvent/membrane interactions, and modifies several of the most important properties of the bilayers, such as the equilibrium area per lipid[19,35].

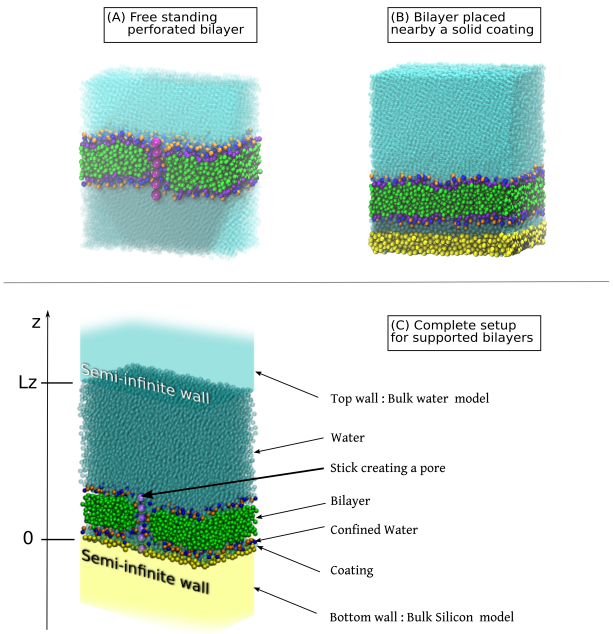


Figure 1: Systems studied in the present work. **(A)** free bilayers, crossed by a stick which is forced to stay vertical, in the middle of membrane. The system is periodic in the three dimensions. **(B)** Bilayer placed close to a disordered coating, either without stick, as in Koutsioubas[13], or with a stick (not shown). The system is periodic in the three dimensions. **(C)** Same as (B), but the system is confined between two walls in the $z$-direction represented by two external potentials $U_{wall}(z)$, and is periodic in the $x$- and $y$-directions only.

A. Koutsioubas has performed simulations of supported 1,2-dipalmitoyl-sn-glycero-3-phosphocholine (DPPC) using the classical Martini by using a support composed of disordered frozen particles[13], as depicted in Fig.1(B). He has shown that the structure of these simulated membranes can be brought in good agreement with neutron reflectivity measurements, in contrast with similar simulations obtained using either the "weak water model" or crystalline supports. Two fundamental parameters have still been imposed to fit experi-

mental data : (1) the area per lipid for the two monolayers were fixed to the liquid or gel phase value for free bilayers; (2) the hydration level of the support, i.e., the confined water amount, between the support and the adsorbed membrane, was constant during the simulation. While such constraints can lead to a good match with experimental data, they do not ensure the equilibration of the system within the chosen model. More generally, different substrate models could be forced by some constraints to fit onto experimental data, even if they would lead to different equilibrium structures. In other words, a substrate model developed with specific constraints might not be transferable to situations where these constraints are released. It is therefore highly desirable to perform SLB simulations with varying hydration levels when developing substrate models.

To go beyond the model in Ref. 13, while preserving its advantages, we propose a relatively smooth support composed of a semi-infinite planar bulk, coated by a thin layer of frozen disordered CG-particles at its surface, as depicted in Fig.1(C). Our model differs from a perfectly smooth wall because of the coating, and from the regular lattice commonly used[16,18,19,33,37,38] because the coating particles are disordered, as in a glassy material. Compared to Koutsioubas's model[13], new ingredients appear. First, the thickness, density and nature of the coating have been varied; second, there is additionally a wall behind the glassy coating interacting with the particle through an external LJ potential. Finally, the equilibrations of the hydration level of the support, and the lipid distribution among the two monolayers were facilitated by the insertion of an artificial pore in the lipid layers, as in Risselada et al.[39](see Fig.1 (A) and (C)). In the following, the utility of the different components of the model are first discussed. Then, the properties of the simulated SLBs are reported, in particular the effect of the long-range external LJ potential. Finally surface neutron reflectivity spectra obtained from the simulations are compared to the experimental ones.

# 2 Methods

To compare our SLB simulated structures with the ones investigated experimentally by neutron reflectometry in Ref. 13, we have used coarse-grained model of DPPC and DAPC in water ($H_2O$ or $D_2O$), and supported on a planar solid representing a silicon wafer with a thin oxidized $SiO_2$ layer at its surface (see Fig. 2).

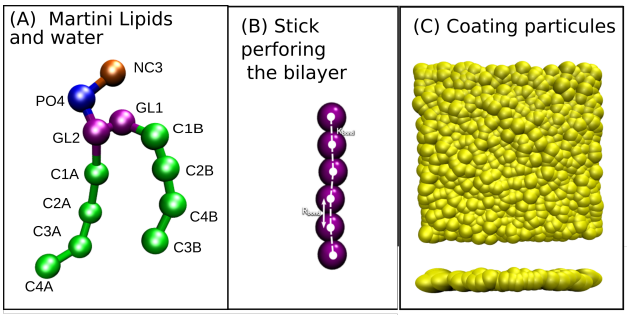


Figure 2: (A) : Coarse-grained model of the phospholipid within Martini. DPPC ($C_{16}$) is depicted here. Each of the two tails of DAPC ($C_{20}$) contains 5 hydrophobic beads, instead of 4 for DPPC. (B) Stick of beads constructed to cross the membrane and to stabilize a pore. (C) Typical coating layer (up view and side view). Here, the sphere diameter is 0.47 nm, as the other particles of the model, representing Martini water density. This diameter was decreased when the coating particle density increased.

## 2.1 Martini-based Model

The simulations are based on the Martini model[28,29]. All CG beads interact pairwise via a Lennard-Jones (LJ) potential with the interaction strengths and cut-offs defined in the Martini model version 2.0. Molecules are decomposed into four families of beads: polar (P), non polar (N), apolar (C) and charged (Q), all with masses of 72 amu and LJ contact radius $\sigma = 0.47$ nm, representing approximately four second-raw atoms and their associated hydrogens.

Water is composed of beads of type `P4`, its LJ parameters ($\epsilon = 5.0$ kJ·mol$^{-1}$, $\sigma = 0.47$ nm) correspond to the solid state region of the LJ phase diagram at typical temperatures, but the cutoff of the potential reduces the long-range attractive part. Freezing is a possible problem at a solid surface which acts as a nucleation site. The use of the usual Martini

anti-freeze water particles, in combination with planar walls was not successful to impede freezing because of a demixing between the traditional and anti-freeze water particles[32]. In the present work, we use solely traditional, non-polar water particles, without anti-freeze particles.

The experimental neutron reflectivity data were available for SLBs of fluid and gel DPPC, so that this work primarily focuses on this lipid. To investigate the effect of chain length, the SLB simulations of DPPC, which fatty acid chains contain 16 carbons, were compared to the ones of 1,2-diarachidoyl-sn-glycero-3-phosphocholine (DAPC), which fatty acid chains contain 20 carbons. The lipid molecules DPPC and DAPC are made out of 12 or 14 CG-beads as depicted on Fig. 2(A). The hydrophobic tails consist of `C1` type particles, the glycerol moiety of `Na` particles of intermediate polarity, and the head group of a negatively charged `Qa` particle for the phosphate group, and a positively charged `Q0` particle for the choline group.

**A hydrophilic pore** was created in the lipidic bilayer to enhance water permeation and lipid flip-flop during the simulations. This pore was stabilized using a "stick" maintained parallel to the $z$-axis and constrained to remain in the lipidic bilayer.

The stick is composed of a new bead type which interacts solely with the tail beads (`C1` type) with a purely repulsive Lennard-Jones potential ($\epsilon = 0.125$ kJ·mol$^{-1}$, $\sigma = 1.0$ nm), chosen so that the distance at the potential minimum ($r_m = 2^{1/6}\sigma \simeq 1.12$ nm) almost corresponds to the cut-off of the LJ potential (1.10 nm).

The tail-repulsive beads are then arranged in a molecule as shown on Fig. 2(B) where the bond force constant is 2000 kJ·mol·nm$^{-2}$, a value slightly higher than the one of the lipid tails. In the $xy$-plane, each stick bead is restrained at the center of the simulation box (force constant of 5000 kJ·mol$^{-1}$·nm$^{-2}$). This ensures that the stick remains parallel to the membrane normal. In the $z$-direction, a harmonic potential is added to maintain the center of mass of the stick close to the center of mass of the lipidic bilayer. The reference position

of the bilayer center is rescaled with the simulation box in the case of pressure coupling in $z$-direction.

The pore stabilized by the stick is hydrophilic and it speeds up water permeation and lipid flip/flop. As shown in Supporting Information, this pore induces perturbation in the local bilayer thickness and area per lipid on a disk of about 6.5 nm of radius (see Figs. S1 and S2, Supporting Information) that was excluded from the the analyses of the supported bilayers. The introduction of the pore in the bilayer also leads to an increase in the total area of the simulated system which was taken into account in the setup of the supported bilayer simulation.

**Substrate Models** containing various ingredients have been compared. The models are composed of a disordered coating of explicit particles, plus an external continuous wall potential depending on the $z$-coordinate $U_{\text{wall}}(z)$ (see Fig. 1(C)).

When compared to experimental SLBs deposited onto silicon wafer, the particular coating represents roughly the oxidized surface of the substrate and its hydration shells. Thicknesses of 0.2 nm and 0.5 nm were tested. The coating introduces some disorder at the interface and prevents water from freezing.

The external wall potential $U_{\text{wall}}(z, \rho^{\text{wall}})$ represents the "semi-infinite" solid (i.e. the bulk silicon wafer) and appears as a continuous potential which strength depends on the $z$-coordinate of the particles and the wall particle density $\rho^{\text{wall}}$:

$$U = \rho^{\text{wall}} \, \frac{2\pi}{3} \, \epsilon_{ij} \sigma_{ij}^3 \left[ \frac{2}{15} \left( \frac{\sigma_{ij}}{z} \right)^9 - \left( \frac{\sigma_{ij}}{z} \right)^3 \right] \tag{1}$$

where $\epsilon_{ij}$ and $\sigma_{ij}$ are the parameters for bead/bead interaction. This 9-3 LJ potential emerges from the integration over a semi-infinite support of homogeneously distributed Lennard-Jones particles at density $\rho^{\text{wall}}$. It is long-range compared to the usual Martini interactions, and should stabilize the adsorption of lipid membranes.

Both the external potential and the frozen particles typically have three degrees of free-

dom : their density, and the two Lennard-Jones parameters $\epsilon$ and $\sigma$. We have restrained the $\{\epsilon, \sigma\}$ couples to the ones of bead types already existing in Martini, in particular the polar `P4` type, and the apolar `Nda` type. Moreover, the coating thickness has been either adjusted to the value used by Koutsioubas (2.0 nm) for comparison purpose, or reduced to 0.5 nm. Indeed, to avoid screening of the wall by the coating particles, the coating thickness was chosen at 0.5 nm, smaller than $3^{1/6}\sigma$ at which the 9-3 potential reaches its minimum.

The types of particles and densities used both for the semi-infinite support and for the coating particles are listed in Table 1.

**Table 1: List of simulations discussed in this work. Densities $\rho^{\mathbf{wall}}$ and $\rho^{\mathbf{coating}}$ are expressed in particle per nm$^3$, and thicknesses in nm. Without bottom and top walls (job IDs 1 to 5), periodic boundary conditions are used in $z$-direction. For the job IDs 10 to 13, two semi-infinite walls are implemented. The Bottom and Top walls are indicated on Fig. 1(C).**

| ID | Temp. | Lipid | Bottom Wall | | Coating | | | Top Wall | |
|---|---|---|---|---|---|---|---|---|---|
| | (K) | | Type | $\rho^{\text{wall}}$ | Type | $\rho^{\text{coating}}$ | Thickness | Type | Density |
| 1 | 323 | DPPC | None | | `Nda` | 8 | 2.0 | None | |
| 2 | | DPPC | | | `P4` | 8 | 2.0 | | |
| 3 | 323 | DPPC | None | | `P4` | 10 to 16 | 2.0 | None | |
| 4 | | DPPC | | | `Nda` | 10 to 16 | 2.0 | | |
| 5 | | DPPC | | | `P4` | 10 to 16 | 0.5 | | |
| 10 | 323 | DPPC | `P4` | 4 to 16 | `P4` | 8 | 0.5 | `P4` | 8 |
| 11 | 295 | DPPC | `P4` | 0 to 16 | `P4` | 8 | 0.5 | `N0` | 1 |
| 12 | 323 | DAPC | `P4` | 4 to 16 | `P4` | 8 | 0.5 | `P4` | 8 |
| 13 | 295 | DAPC | `P4` | 0 to 10 | `P4` | 8 | 0.5 | `N0` | 1 |

## 2.2 Simulation Protocol

The simulation protocol is summarized here, and described in detail in Sect. S1 of the Supporting Information. All simulations were performed using Gromacs (2016.3 or 2018.5) [40]. The parameter set was the *common* one from de Jong et al. [41], a choice based on a previous careful testing of the energy conservation for lipid bilayer simulations using Martini along with Gromacs [42]. The initial conformations were generated using Packmol [43]. Preliminary simulations have been performed to describe the free bilayers, either without a pore or with

the pore stabilized by the stick (Fig. 1-A). They made it possible to describe the perturbation of the bilayer by the pore in the absence of substrate (see Fig. S1, Supporting Information).

For the actual SLB simulations (see Figs. 1B and 1C), an amorphous coating made of beads was generated with the same in-plane dimensions as the final state of the free bilayers, with the desired coating type and densities. The positions of the coating particles are extracted from bulk Martini water simulation at 323 K. The initial hydration was set to about 3.6 water beads per lower lipid using a translation of the membrane relative to the substrate before the beginning of the simulation. These initial coordinates were used for modeling the substrate without and with the wall potentials (Figs. 1B and 1C respectively). For the simulations without any wall potential (Fig. 1B), the system is periodic in the three dimensions. For those with wall potentials (Fig. 1C), the system is confined between two walls in the $z$-direction represented by two external potentials $\mathrm{U_{wall}(z)}$, and is periodic in the $x$- and $y$-directions only. The wall representing the substrate was described with a density $\rho^{\mathrm{wall}}$ varying from 0 to 20 particle per $\mathrm{nm}^3$, and the bead type `P4` or `Nda` .

After equilibration steps, the SLBs were simulated for 20 $\mu$s in the $NAP_zT$ ensemble with a pressure $P_z = 1$ bar obtained by a Parrinello-Rahman barostat with compressibility of $3 \times 10^{-4}$ bar or with a Berendsen barostat with a pressure coupling time of 3 ps and a compressibility of $3 \times 10^{-4}$ bar.

## 2.3 Analysis of Trajectories, Calculation of Neutron Reflectivity Spectra

VMD[44] was used to visualize the trajectories and to produce 3D renderings. To analyze the impact of the artificial pore in the membrane (see Fig. S1, Supporting Information), the local measurement of characteristic membrane properties such as the area per lipid, thickness and lipid order parameter was made possible with a self-modified version of FatSlim[45,46]. This program represents the lipids as a bead for the head and a 3-dimensional vector for the tail orientation. It estimates a local normal for each lipid. This information permits membrane

leaflet identification and the computation of local membrane properties for each leaflet.

The amount of hydration water of the proximal leaflet ($n_{\mathrm{W}}^{\mathrm{p}}$), i.e. the number of water beads between the substrate coating and the lipid bilayer, was computed using Gromacs analysis tools `gmx select`, which allows the measurement of physical quantities and the dynamical selection of beads to analyze particles matching user-defined conditions. For this analysis, a cylinder centered on the membrane pore with a radius of 6.5 nm and spanning the whole simulation along the z-axis was removed from the simulation trajectories (for a justification of this excluded zone, see the analysis of the local impact of the pore in the SI). This water amount was either rescaled by the number of lipids in the proximal leaflet ($n_{\mathrm{L}}^{\mathrm{p}}$), or it was converted into a thickness of confined water ($t_{\mathrm{W}}^{\mathrm{p}}$) using

$$t_{\mathrm{W}}^{\mathrm{p}} = \frac{n_{\mathrm{W}}^{\mathrm{p}}}{d_{\mathrm{W}}\ a_{\mathrm{L}}^{\mathrm{p}}\ n_{\mathrm{L}}^{\mathrm{p}}}, \tag{2}$$

where $d_{\mathrm{W}}$ is the water density, arbitrarily fixed at the bulk water value of 8.4 beads/nm$^3$, and $a_{\mathrm{L}}^{\mathrm{p}}$ is the area per lipid in the proximal leaflet. We defined the leaflet density asymmetry ($\Delta_{\mathrm{L}}^{\mathbf{pd}}$), using the number of lipids in the proximal and distal leaflets ($n_{\mathrm{L}}^{\mathrm{p}}$ and $n_{\mathrm{L}}^{\mathrm{d}}$ respectively) :

$$\Delta_{\mathrm{L}}^{\mathrm{pd}} = \frac{2\left(n_{\mathrm{L}}^{\mathrm{p}} - n_{\mathrm{L}}^{\mathrm{d}}\right)}{(n_{\mathrm{L}}^{\mathrm{p}} + n_{\mathrm{L}}^{\mathrm{d}})}. \tag{3}$$

Averages and errors on $t_{\mathrm{W}}^{\mathrm{p}}$ and $\Delta_{\mathrm{L}}^{\mathrm{pd}}$ were calculated on the last 10 $\mu$s of the 20 $\mu$s-long simulations.

The formalism used for the computation of the neutron reflectivity spectra is given in Section S4.1 of the Supporting Information. Our home-made in-line python script [47] performs a similar analysis as the graphical user interface presented in Ref. 12 and other works with different numbers of lipidic layers [48,49]. In a first step, a self-modified version of MDAnalysis [50,51] was used to measure beads density along the membrane main axis in the relevant part of the simulation. In more details, for the 2000 MD-snapshots in the last 2 $\mu s$ of the 20 $\mu s$ simulation, the density profile of the different beads is computed outside a cylinder

of 6.5 nm that span the whole box along the $z$-axis (to avoid the part of the membrane perturbed by the pore). The density profile of the system is then time-averaged providing $\rho(z)$ for each bead type. Since an artificial water layering is observable in the vicinity of the bulk water top-wall, and the density profile in the domains $z \geq 10$ nm and $z \leq 0.5$ nm has been removed and replaced with idealized densities described below. Noticeably, the matching between experimental and simulation data can be slightly improved by introducing in the profiles the possibility of an imperfect coverage of the substrate by the bilayer[12,13]. To account for a ratio $x_{\mathrm{W}}$ of the substrate area covered by water instead of bilayer, the bead density profiles obtained from the MD simulation were multiplied by $1 - x_{\mathrm{W}}$, and the corresponding quantity was added to the water profile. Optimum values of $x_{\mathrm{W}}$ are around 2% and 5% for the fluid and gel DPPC SLBs respectively (see Fig S5 in SI).

Once the MD bead density profiles have been calculated, the Scattering Length Density (SLD) profile is derived by a linear combination of the density profiles of the beads, weighted by the scattering length $b$ of the atoms they represent. The lengths $b$ are taken from Ref. 13, see Table S1, Supporting Information. The SLD profile has been finally convolved by a Gaussian function of standard deviation of 0.16 nm. This convolution mimics the fluctuations of density profiles which are not taken into account in the simulations. In particular, in the experiments, the position fluctuations of the membrane around its planar average position are expected to be larger than in the simulations. To represent the bulk part of the substrate and the solvent not modeled explicitly in the system, a layer of $SiO_2$ and Si are added below the coating with SLD values of 3.47 and $2.07\times10^{-6}$ Å$^2$ respectively. The thickness and roughness of Si and $SiO_2$ layers are set manually to increase the matching between simulated and experimental reflectometry curves for the bare substrates (see Fig S4). Typical values correspond to a 1.1 nm-thick $SiO_2$ layer with a roughness of 0.5 nm, and a 10 nm-thick Si layer with no roughness.

In a third step, the specular reflectometry curves are derived following the formalism described in Sect. S4.1 in the Supporting Information. It is based on the Abeles matrix method

for a model of reflecting layer stack with different thicknesses, SLDs, and roughnesses[52].

Finally, to measure the discrepancy between experimental and modeled reflectivity curves, a commonly used metric $\chi$ is[12]:

$$\chi^2 = \frac{1}{(N\ -\ 1)} \sum_{i=1}^{N} \frac{[\ R_{\mathrm{exp}}(q_i)\ -\ R_{\mathrm{sim}}(q_i)\ ]^2}{[\ \sigma_{\mathrm{exp}}(q_i)\ ]^2}, \tag{4}$$

where $N$ is the number of data point in the experimental curve, $R(q_i)$ is the reflectivity at the momentum $q_i$, and $\sigma(q_i)$ its standard deviation.

# 3 Results and Discussions

This Section first presents our model development, and justifies the different elements of our model. Then, the structure and fluctuations of the simulated SLBs based on our composite model with long-range interactions are investigated.

## 3.1 SLB Model Development

In this Section, SLB simulations are presented for models of increasing complexity. All the substrate models contain a coating layer of disordered particles to avoid crystallization. We investigated in particular the thickness of confined water.

The first model is a frozen layer of solvent, as in Ref. 13 (Sect. 3.1.1). Using this simple case, we first justify the necessity to enable a variable hydration level during the simulation when comparing substrate models. Then, we show that this simple substrate is not attractive enough to obtain strongly adsorbed fluid SLBs. The second substrate model (Sect. 3.1.2) is similar, but the nature and the density of the coating layer is varied so as to modulate the short-range bilayer/substrate interaction. In the third model, a long-range wall potential is added (Sect. 3.1.3). This permits to fine-tune the hydration level of the membrane.

### 3.1.1 Impact of Membrane Poration

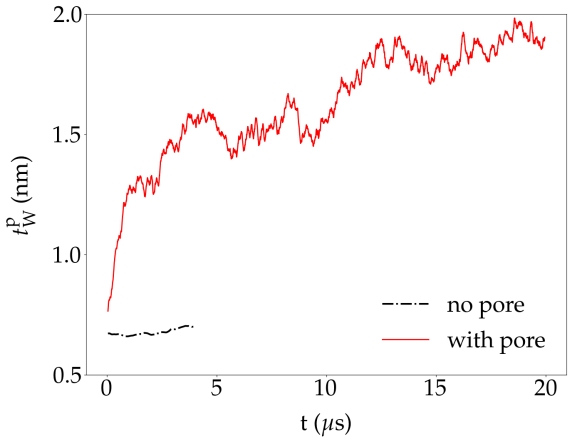


Figure 3: Confined water thickness ($t_W^P$) as a function of simulation time (t) for fluid DPPC membrane,with and without the artificial pore. The substrate model is a frozen disordered `Nda` coating (thickness of 2.0 nm and density of 8 beads per nm$^3$). The simulation without pore has been stopped after 4 $\mu$s. The values plotted are sliding averages over 1000 values corresponding to time windows of 100 ns. Typical standard deviations around these averages are 0.1 nm for the simulation with the pore. They are negligible for the simulation without the pore.

The substrate model from Koutsioubas[13] is composed of a 2-nm thick frozen layer of disordered particles. It made it possible to carry out SLB simulations whose structures are in good agreement with neutron reflectometry. But these simulations were performed under fixed areas per lipid for the proximal and distal leaflets, and also an ad-hoc quantity of hydration water (the water confined between the membrane and the substrate). In a first step, we have checked whether these simulations are stable in time when these constrains are released thanks to an artificial pore in the membrane. Fig. 3 illustrates the impact of the presence of the pore on the time-evolution of confined water thickness ($t_W^P$), for DPPC fluid bilayers supported on a 2 nm-thick coating of `Nda` beads. A simulation without pore was performed during 4 $\mu$s, as in Ref. 13, and a simulation with the pore was performed for 20 $\mu$s (1 and 2 in Table 1). Two different behaviors are observed. When the membrane has no pore, it is almost impermeable and the amount of water trapped between the bilayer

and the substrate is kept almost constant, at least at the timescale of the simulation. When a pore is included in the membrane, the water is able to flow through the membrane and the confined water thickness increases with time ; no convergence towards an equilibrium is observed, even after the 20 $\mu$s of the simulation. Clearly, the membrane is not maintained in the initial position when the hydration constraint is released and the final simulated structure no longer matches with the experimental neutron reflectivity data. Changing the substrate beads to more hydrophilic ones (`P4` type) does not change the global behavior: the membrane significantly moves away from the substrate.

A slab of frozen `Nda` or `P4` particles is therefore not attractive enough to impose the membrane binding observed experimentally. Despite the short-range attractive forces between the substrate and the membrane included in Martini force field, repulsive forces between the fluid membrane and the substrate favor a drift of the membrane away from the substrate. In the absence of surface tension, the presence of the frozen substrate restrains the membrane position fluctuations, which is associated with a long-range repulsive pressure proportional to $(k_BT)^2/(K_cD^3)$, where $K_c$ is the bending modulus of the bilayer and $D$ the average membrane-substrate distance[1,53]. If the attractive force is not strong enough, an unbinding transition can occur[54].

Moreover, in the simulations without the pore, the symmetry in the number of lipid in each leaflet is practically constrained since flip/flops do not occur. By contrast, it was shown in experimental works that for SLBs in fluid phase, the flip/flop can lead to equilibration within minutes[55]. Since compositional asymmetry is correlated to the stress in the monolayers[56,57], a constraint on a *symmetrical* lipid composition may impose mechanical stress in the simulated SLBs.

These conclusions have motivated us to develop SLBs simulations where (i) the membrane hydration level is not constrained during the simulation, (ii) the lipidic membrane is more strongly attracted by the substrate. Two solutions were tested to favor membrane adhesion. The first one was an increase of the particle density in the coating, which lead to a stronger

short-range attraction (Sect. 3.1.2). The second was the addition of a semi-infinite LJ-bulk below the coating, via an external potential (Sect. 3.1.3) .

### 3.1.2 Increasing Short-Range Forces : a Difficult Control on Fluid Membrane Binding

To increase the attractive forces between the membrane and the substrate with minimal modification in the simulation protocol, we tested two modifications of the coating model : either an increase of the density $\rho^{\text{coating}}$, or a change of the bead type (simulations 3 to 5 of Tab. 1). The simulations using `Nda` coating particles (simulation 4 in Tab. 1, with $d > 10$) did not yield SLB systems, because some hydrophobic tails of the lipids had adsorbed on the coating, disrupting the membrane. Some simulations using `P4` coating particles and a thickness of 2 nm (simulation 3 in Tab. 1) were also unstable, because the adhesion of the membrane on the coating was so strong that the pore in the membrane was no longer stable, resulting in unphysical structures.

Most simulations with `P4` coating particles and a thickness of 0.5 nm (5 in Tab. 1) have yielded the expected SLB structures with a pore, and these were stable for the 20 $\mu$s of our simulations. Fig. 4 illustrates the time-evolution of the confined water thickness ($t_{\text{W}}^{\text{p}}$) for the successful simulations. It turned out that increasing the coating density was not efficient to

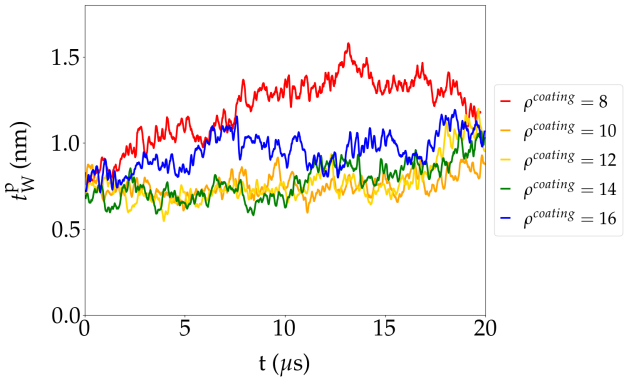


Figure 4: Confined water thickness ($t_{\text{W}}^{\text{p}}$) as a function of simulation time (t) for different densities of the coating ($\rho^{\text{coating}}$) in bead·nm$^{-3}$, for fluid DPPC SLB at 323 K. The statistical analysis is the same as in Fig. 3.

rationally fine-tune the equilibrium confined water thickness for our fluid SLB simulations. The SLD density profiles are not much influenced by the coating density. The matching of the calculated reflectivity curves with experimental even worsens when $\rho^{\text{coating}}$ is increased (see Fig. S6).

To conclude, increasing the coating density might favor the spontaneously adsorption of the bilayer when using the `P4` beads for the coating, however, this model turned out to be unpractical. Within our tentatives, such a model was too poorly flexible to adjust simulated structures to the ones obtained from neutron reflectivity data. We interpret this results as the difficulty to compensate the long-range repulsion between the membrane and the wall using strong short-range forces. Therefore, in the following, we have included a long-range attraction between the substrate and the membrane.

### 3.1.3 Adding Long-Range Attraction to Tune Hydration Level

In the following, the substrate model was completed by an external LJ-potential which mimics the interactions between the bulk substrate and the adsorbed membrane. For the lipid heads, at a distance larger than $\simeq 0.5$ nm relative to the wall, this potential leads to long-range attraction forces which are usually neglected in the Martini model. In addition to the external LJ-potential, the thin disordered coating present in former models is kept, to prevent the system from freezing, and to mimic some nanoroughness of the substrate surface (see Fig. 1(C)).

The simulations performed with the LJ wall potentials (simulations 10 to 12 in Table 1) produced regular SLB structures [1]. Fig. 5 illustrates the confined water thickness $t_{\text{W}}^{\text{p}}$ for the fluid DPPC simulations (10 in Table 1). It converges with time around an equilibrium value which decreases when the prefactor of semi-infinite wall potential increases. For the lowest wall density ($\rho^{\text{wall}} = 4$ part$\cdot$nm$^{-3}$), the membrane position fluctuates at time-scale of

[1] Except for the extreme case of a wall density of 50 beads per nm$^3$. This case was trapped in a metastable state, where a big water droplet was trapped below the membrane. The diffusion of the water trough the pore was impeded because the membrane around the pore was tightly bound to the substrate. We therefore stopped this irrelevant simulation.

the order to the simulation time, so that the equilibrium position of the membrane is not known precisely. For wall densities between 6 and 16 part.·nm$^{-3}$ the model is flexible with various hydration levels achievable, and with an easy fine tuning. Some curves represented on

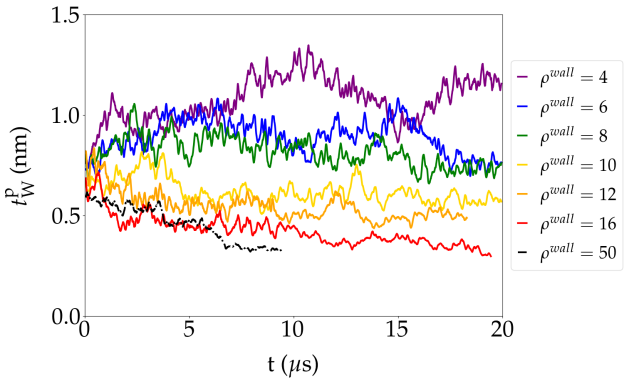


Figure 5: Confined water thickness ($t_W^P$) as a function of simulation time (t) for different densities of the semi-infinite wall potential ($\rho^{wall}$), in part.·nm$^{-3}$), for fluid DPPC SLBs at 323 K. The statistical analysis is the same as in Fig. 3.

Fig. 5 show variations at the $\mu$s time scale. We have interpreted these variations as relatively fluctuations around a single average value, and have chosen the last 10 $\mu$s of simulations to calculate the average water thicknesses. Interestingly, Vishnyakov and co-workers recently reported all-atom SLBs' simulations with two possible distinct hydration levels of SLBs : one with molecularly thin (less than 0.5 nm) and another at 2 to 3 nm thick hydration layers[27]. In our simulations, we do not find the trace of the existence of these two co-existing equilibrium configurations. A complete search for these is beyond the scope of the present work.

To conclude, we have ended up using a composite model for the SLBs, where the various ingredients play different roles : the substrate external potential favors membrane adsorption, the substrate coating avoids crystallization, and the pore in the membrane allows for a varying hydration level and a membrane asymmetry.

## 3.2 Properties of the SLBs

We present here further results on the model developed in Sect. 3.1.3. The structure of the SLBs is investigated for different Hamaker constants. Then, the comparison with experimental reflectometry data provides a way to optimize the parameters of the substrate model. Differences observed between gel and fluid SLB simulations are briefly discussed.

### 3.2.1 Structure Asymmetries

The MD simulations provide details on the molecular structure of the SLBs. In particular, Fig. 6 shows the density profiles of various bead types projected in the $z$-direction for the SLBs of fluid DPPC (with three increasing densities among the simulations 10 and 11 in Table 1).

When a `P4` top wall is used, water layering is clearly observed for $z \geq 10$ nm, in the vicinity of the top wall, i.e. the perfectly flat boundary representing bulk water, Since this structuration lead to water freezing at 295 K, we have replaced the top hydrophilic wall by a hydrophobic wall of type `N0`. Then, no layering effect was observed. Anyway, the irrelevant part of the system $z \geq 10$ nm was not included in further analysis, and in the following we focus on the relevant part ($z \leq 10$ nm).

For the lowest wall densities, the density profiles of the lipid heads, tails and nearby water are not significantly altered from the free-standing DPPC membranes. For the fluid SLBs, with increasing wall density, the confined water becomes thinner, and more structured. The proximal leaflet is also slightly more structured. For wall densities larger than 8 part$\cdot$nm$^{-3}$, two peaks appear in the head density profile, one for the glycerol (`GL1` and `GL2` beads), and one for the zwitterions (`NC3` and `PO4` beads) (See also Fig. S7). But the structuration remains much less pronounced than for density profiles obtained with SLB simulations using either flat substrate, or ordered particles[13].

In this respect, the density profiles of our coarse-grained model are similar to the ones reported for all-atom simulations of phospholipid bilayers adsorbed on a hydrophilic crystal

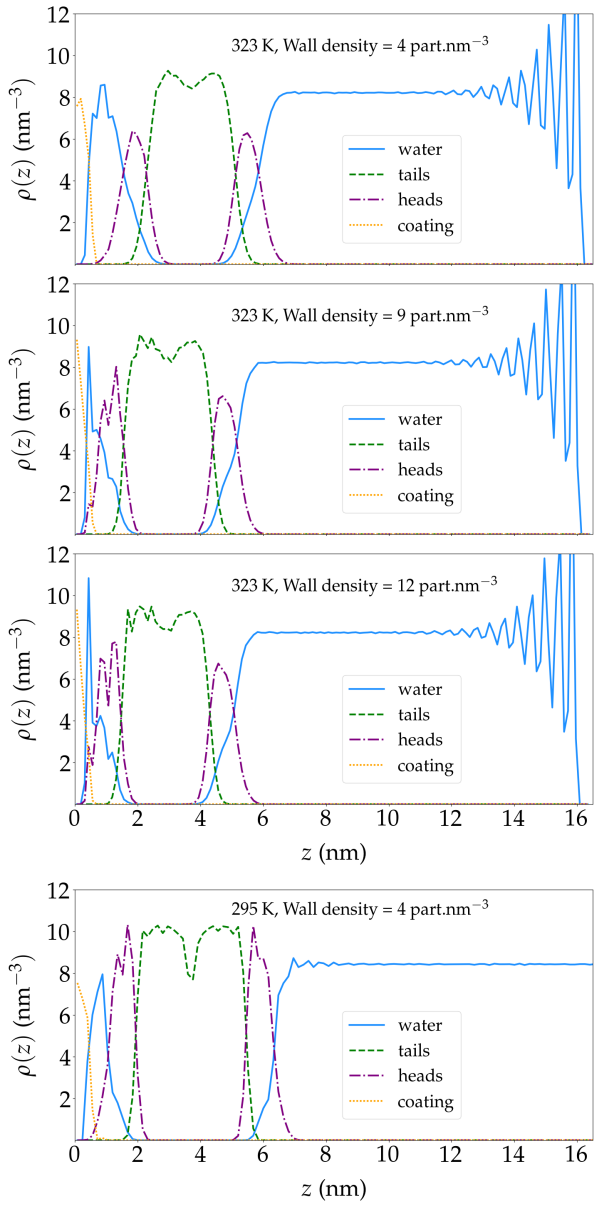


Figure 6: Particle density profiles $\rho$ along the coordinate $z$ normal to the substrate, in the SLB simulations of DPPC with a `P4` wall ("tails" labels `C1` beads, "heads" labels the choline, phosphate and glycerol beads). The top wall is either a `P4` at density 8 part·nm$^{-3}$, or a `N0` at density 1 part·nm$^{-3}$ for the temperatures 323 K and 295 K respectively.

of cellulose : they show a moderate structuration of both the confined water layer, and the proximal leaflet[20]. The distal leaflet is less perturbed.

Fig. 7 illustrates the relative lipid number differences $\left\langle \Delta_{\mathrm{L}}^{\mathrm{pd}} \right\rangle$ obtained for SLBs of DPPC and DAPC in the fluid phase (simulations 10 and 12 in Table 1). For large substrate/membrane

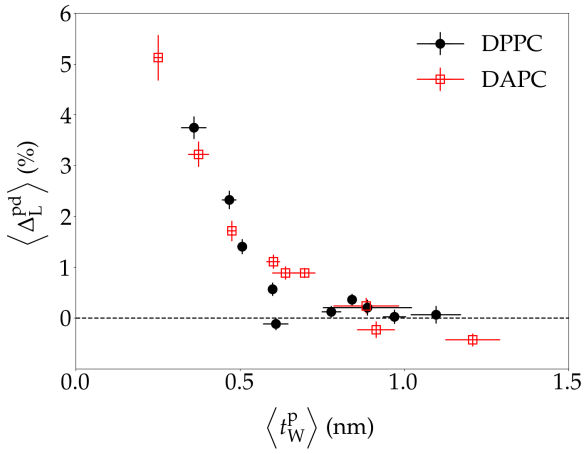


Figure 7: Relative lipid number difference in the two leaflets $\langle \Delta_L^{pd} \rangle$ as a function of the confined water thickness $\langle t_W^p \rangle$, for the fluid SLBs of DPPC and DAPC (323 K).

distances, as expected, no lipid density asymmetry is measured. When the membrane is in contact with the substrate, a lipid number asymmetry of about 5% can be measured, with a higher density of lipids in the proximal leaflet, in qualitative agreement with previous studies of SLBs[16,18,19,36]. Contrarily, for bilayers in the gel phase, the proximal and distal leaflets have similar structures (see Fig.6), with no density differences in the two leaflets.

To summarize, we observe a correlation between a membrane asymmetry and the hydration level. In the following, the control of the hydration level through the model parameters is investigated.

### 3.2.2 Varying Hydration Level

As seen previously, the hydration level, or confined water thickness $\langle t_W^p \rangle$ varies depending on the simulation parameter $\rho^{wall}$ (see Figs. 5 and 6). In the following, we investigate in more details the relationship between the two by comparing our simulations to simple analytical models of membrane/substrate interactions.

Fig. 8 summarizes the averaged confined water thickness $\langle t_W^p \rangle$ obtained from the simulations 10 to 13 in Table 1. The two frames contain the same simulation results, but two

different models to fit them. For all systems, the equilibrium confined water thickness de-

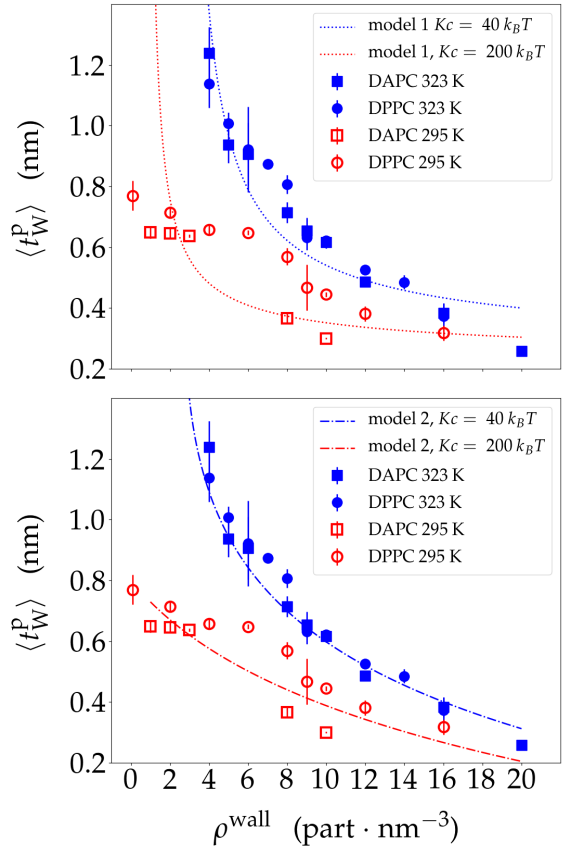


Figure 8: Equilibrium confined water thickness $\langle t_W^P \rangle$ as a function of wall density $\rho^{wall}$, for the SLB simulations of two lipids at two temperatures. Top : The lines correspond to fits using Eq. 5 with 4 parameters. Bottom : The lines correspond to fits using Eq. S16, emerging from Eq. 7 with 6 parameters. Two of these parameters are the bending moduli $K_c$, fixed at 40 $k_BT$ and 200 $k_BT$ for the fluid and gel phases respectively[58–61].

creases as the wall density is increased, until the membrane almost touches the substrate coating. At 323 K, the hydration levels are similar for the two lipids, despite the longer tail of DAPC relative to DPPC. This result is encouraging concerning the transferability of the substrate model for different lipids or multicomponent SLBs, but such a study is beyond the scope of the present work

Interestingly, the hydration curve strongly depends on temperature. In the regime of strong wall attraction ($\rho^{wall} \geq 10$ part.nm$^{-3}$), the gel and fluid phases are both strongly adsorbed with a very thin water layer, of 0.5 nm or less. For lower wall attraction ($\rho^{wall} \leq 8$ part.nm$^{-3}$),

the gel and fluid phases behave differently : while in the gel phase the membrane remains very close to the substrate, in the fluid phase it begins to separate from the substrate, with a water thickness increasing up to 2 nm.

Direct comparison of the simulation data in Fig. 8 with experiments is tricky because the Hamaker constant cannot be easily tuned experimentally. But the present simulations match the following experimental observations: for single supported bilayers, both in gel and fluid phase, and for different zwitterionic lipids, the confined water thickness is almost constant and always lower than 1 nm[1,6,13]. Indeed, for $\rho^{\text{wall}} > 8$ part·nm$^{-3}$, corresponding to realistic values for silicon oxide (see below for more details on how to choose the best density to fit NR data), both gel and fluid lipids lead to similar confined water thicknesses. In contrast, for $\rho^{\text{wall}} < 8$ part·nm$^{-3}$, the simulations may correspond to the experimental case of a floating bilayer, where temperature clearly impacts the confined water thickness[6,62].

This variety of behaviors is the result of a balance between different pressures acting on the membrane : the long-range attraction from the wall, the short-range hydration repulsion, electrostatic and Lennard-Jones forces[54]. We compare here the simulations to two phenomenological models describing a membrane in an effective potential $U_{\text{eff}}(z)$. In the first model[63], the total free energy of the membrane is approximated by two contributions :

$$U_{\text{eff}}(z) \simeq -\frac{A}{12\pi z^2} + c_H \frac{(k_B T)^2}{K_c} \frac{1}{(z - z_0)^2}. \tag{5}$$

The first term is the bare attractive potential energy, approximated by a $1/z^2$ term, dominant at short distance. $A$ is the Hamaker constant that is involved in the interaction with the substrate. We assume that $A$ is proportional to $\rho^{\text{wall}}$ : $A = \alpha\ \rho^{\text{wall}}$. The second term in Eq. 5 is an entropic repulsion, taking into account the renormalization of the interaction by membrane fluctuations, as described by Helfrich[53]. $c_H$ is Helfrich's numerical prefactor and $K_c$ the membrane bending modulus. To account for hydration repulsion, the hard wall is shifted to the position $z = z_0$, with $z_0$ a characteristic length of the order of the hydration

length ($z_0 \sim 0.5$ nm). The thickness at which this effective potential reaches its minimum is

$$t_{\mathrm{W}}\left(\rho^{\mathrm{wall}}\right) \simeq z_0 \frac{\left(\rho^{\mathrm{wall}}\right)^{1/3}}{\left(\rho^{\mathrm{wall}}\right)^{1/3} - \left(\rho_{\mathrm{u}}^{\mathrm{wall}}\right)^{1/3}}, \tag{6}$$

where $\rho_u^{\mathrm{wall}} = \left(k_B T\right)^2 / \left(12\pi c_H \alpha K_c\right)$ is the unbinding density. At large density $\rho^{\mathrm{wall}} \gg \rho_{\mathrm{u}}^{\mathrm{wall}}$, the potential is dominated by the van der Walls attractive part and $t_W \sim z_0$. When $\rho^{\mathrm{wall}}$ tends to $\rho_u^{\mathrm{wall}}$, the bilayer unbinds[64].

The equilibrium thickness $t_{\mathrm{W}}$ (Eq. 6) emerging from this simple potential is compared to the water thicknesses $\langle t_{\mathrm{W}}^{\mathrm{p}} \rangle$ obtained from the various simulations in Fig. 8 (top). For this numerical comparison, the bending moduli $K_c$ have been fixed at typical values: 40 $k_B T$ and 200 $k_B T$ for the fluid and gel phases respectively[58–61]. Then two parameters have been adjusted, $z_0 = 0.2$ nm (equal for both gel and fluid phases) and $\rho_{\mathrm{u,\,fluid}}^{\mathrm{wall}} \simeq 2.5$ part.nm$^{-3}$. The ratio of bending moduli yields then $\rho_{\mathrm{u,\,gel}}^{\mathrm{wall}} \simeq 0.8$ part.nm$^{-3}$. The top of Fig. 8 shows that the simulations of the SLBs is in a qualitative accordance with Eq. 5 for the fluid SLBs. The analytical model and the simulations also show that the gel SLBs remain close to the substrate in a wide range of Hamaker constants. But the agreement between the model and the simulations is less good for SLBs in the gel phase. In particular, Eq. 5 predicts an unbinding of both gel and fluid membranes at low values of Hamaker constant (i.e. low $\rho^{\mathrm{wall}}$). In the simulations, the bilayers in the gel phase remain adsorbed. We attribute this discrepancy to the short-range attractive forces between the substrate and the hydrated lipid bilayer, which are present in the simulations, but absent in Eq. 5. To take into account these forces, a second model for $U_{\mathrm{eff}}(z)$ is proposed:

$$U_{\mathrm{eff}}(z) \simeq \epsilon \left[ \left(\frac{z_0}{z}\right)^6 - \left(\frac{z_0}{z}\right)^4 \right] + \frac{A_2}{z^2}, \tag{7}$$

$$A_2 \simeq c_H \frac{(k_{\mathrm{B}} T)^2}{K_c} - \frac{A}{12\pi} \tag{8}$$

where the short-range interaction of the membrane with the thin coating (the first layer of

beads) is represented as a single $6-4$ Lennard-Jones potential (with $\epsilon$ and $z_0$ as units of energy and length, different from the simulation MARTINI parameters). The $1/z^4$ attractive part corresponds to the integration of a usual $1/r^6$ van der Waals interaction over a thin layer. The $1/z^6$ repulsive interaction is chosen for mathematical convenience. The analytical description of the corresponding water thickness (reported in Supporting Information, Eq. S16) has been fitted onto the simulation data, as depicted in the bottom of Fig. 8. Incorporating the attraction at short distances improves the match between the model and the simulation results for the gel phase in particular, since it accounts for the presence of stable gel SLBs for low wall density ($\rho^{\text{wall}}$). The price to pay is the presence of two additional parameters in this second model.

In conclusion, the hydration level can be tuned in the simulation, and the comparison with two phenomenological models supports the interpretation that the water hydration layer increases for SLBs in the fluid phase because of the membrane fluctuations.

### 3.2.3 Neutron Reflectivity Curves of DPPC SLBs

To become more quantitative in comparing the simulations with experiments, we have calculated the neutron reflectivity curves emerging from the simulated structures. Indeed, the reflectivity and scattering curves of neutrons or X-rays provide a demanding test for membrane simulation[12,13,65]. Since our substrate model of Fig. 1(C) contains a flexible parameter to simulate SLBs with various hydration levels, it becomes possible to minimize the difference between experimental and simulation reflectivity curves, quantified by the metric $\chi$ (Eq. 4) with respect to the wall density $\rho^{\text{wall}}$.

Unfortunately, the calculation of the SLD profiles from the MD-trajectories involves choices concerning other numerical parameters describing the substrate layers (thickness and roughness), which have a strong impact on the details of the SLD profile in the region of the confined water layer. To circumvent this difficulty, the parameters for the Si, $SiO_2$ layers and the coating beads were adjusted for the bare hydrated substrate (see Fig. S4,

Supporting Information), and kept constant for the rest of the studies.

In the second step, the calculation procedure was extended to the case of SLB simulations, keeping all parameters fixed, leaving $\rho^{\text{wall}}$ as the only degree of freedom. The impact of the wall density $\rho^{\text{wall}}$ on the calculated reflectivity curves was then investigated.

**Fluid SLBs** Three typical SLD profiles and the corresponding reflectivity curves for hydrogenated DPPC SLBs in $D_2O$ are plotted for three different wall densities in Fig. 9. As

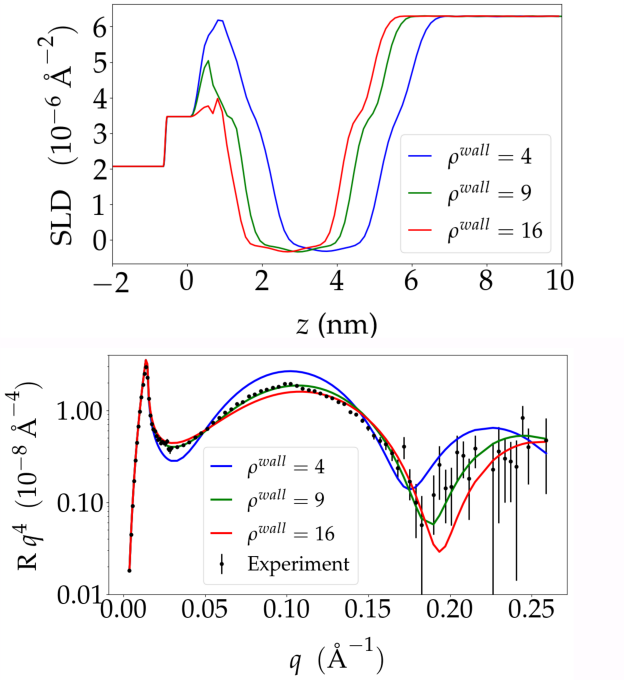


Figure 9: Top: Scattering Length Density profiles from MD simulation of the fluid DPPC SLBs at 323 K, with $\rho^{\text{wall}} = 4, 9, 16$ part·nm$^{-3}$. Bottom: Corresponding reflectivity curves, compared to experimental data from Ref. 13 for the same temperature, hydrogenated lipids and deuterated water. For an estimate of the deviations of the reflectivity curves in time, see Fig. S8.

expected from Fig. 6, the peak in the SLD nearby $z = 0$ (corresponding to the confined heavy water) is less pronounced for increasing wall densities. Both the maximum and the broadness of this peak have a strong impact on the reflectivity curves at larger momentum $q \geq 0.1$ Å$^{-1}$. Among the tested wall densities, $\rho^{\text{wall}} \simeq 9$ part·nm$^{-3}$ minimizes the metric $\chi$ (see Fig. S5 in the Supporting Information). In the following, we discuss the physical relevance of such a

value. First, this density is close to the water bulk density (8.2 part·nm$^{-3}$), and to the total system density, and is therefore reasonable. Second, the strength of this potential can be compared to typical Lennard-Jones interactions with solid supports, measured in terms of Hamaker constants. For example, the interaction of the wall with a semi-infinite of volume of bulk water is detailed in the Supporting Information (see Eq. (S5)). Using our Martini parameters ($\rho_{\text{wall}} = 9$ part.nm$^{-3}$, $\rho_{\text{water}} = 8$ part.nm$^{-3}$, $\varepsilon = 5$ kJ.mol$^{-1}$, $\sigma = 0.47$ nm), and according to Eq. (S5), we estimate a Hamaker constant of 170 kJ.mol$^{-1}$.m$^{-2}$, or 280 eV.m$^{-2}$, i.e. about one order of magnitude larger than the typical Hamaker constant measured for the interaction between solid oxides and water through vacuum[66]. Values of $\rho_{\text{wall}}$ between 1 and 10 part.nm$^{-3}$ appear as physically meaningful to represent typical oxide substrates.

Given the coarse-grained model of the simulations, a quantitative matching of experimental/simulation potential energies is not expected. Preciser models are needed (e.g. Ref. 67). Even more, for our simulations, the $\rho^{\text{wall}}$ optimizing neutron reflectivity matching is expected to be system-size dependent. Indeed, since the membrane fluctuations increase with the system size, the force needed to counterbalance the corresponding repulsion should also increase with system size. Moreover, the optimal parameters for the substrate/membrane interaction may vary in different CG-systems. In particular, entropic and hydration forces depend on the membrane phase[68]. Therefore, the optimization of $\rho^{\text{wall}}$ is discussed again for the case of gel DPPC SLBs.

**Gel SLBs** In Fig. 10, three typical SLD profiles and the corresponding reflectivity curves for the gel DPPC SLBs are plotted, for hydrogenated lipids and deuterated water. All the SLD substrate parameters have been fixed at the same values as for the SLBs in the fluid phase. For the gel phase, the agreement of the experimental and simulation reflectivity curves is not as good as for the fluid phase, even when adjusting the parameter describing the amount of coverage (5%). Since the discrepancy becomes significant for $q \geq 0.12$ Å$^{-1}$ (i.e. lengths smaller than 5 nm), it may originate in the limitations of the Martini model

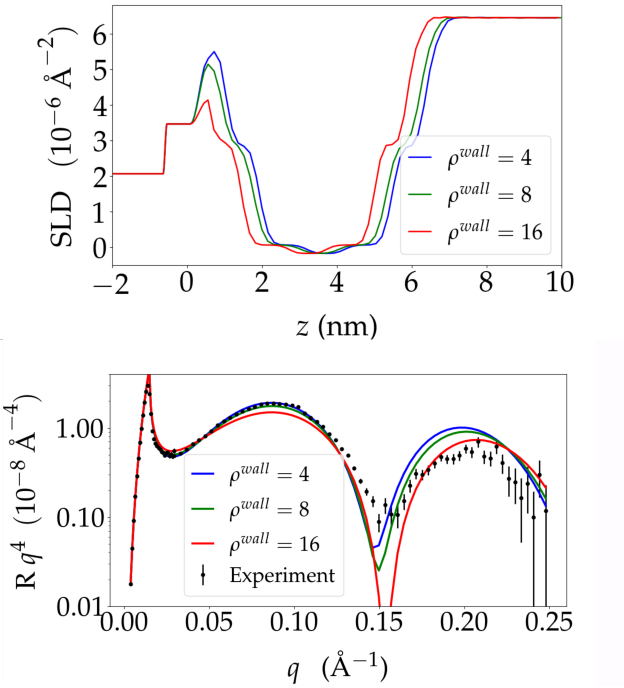


Figure 10: Top: Scattering Length Density profiles from MD simulation of the gel DPPC SLBs at 295 K, with $\rho^{\text{wall}} = 4, 8, 16$ part·nm$^{-3}$. Bottom: Corresponding reflectivity curves, compared to experimental data from Ref. 13 for the same temperature, hydrogenated lipids and deuterated water.

to reproduce some details of the DPPC gel structure, in particular the lipid tilt [13]. Indeed, the 1-4 level of coarse-graining provided by the Martini model does not guarantee enough precision for the membrane thickness. Similar limits appear for Martini simulations of 1,2-distearoyl-sn-phosphatidylcholine (DSPC) monolayers [65].

Because of the inaccuracy of the simulation data, and because of the saturation of $\langle t_{\text{W}}^{\text{p}} \rangle$ as a function of $\rho^{\text{wall}}$, the optimization of the density $\rho^{\text{wall}}$ is less reliable in the case of gel phase. We estimate that the best matching is for $\rho^{\text{wall}} \leq 9$ part·nm$^{-3}$.

To summarize, optimizing our substrate Martini model including both a long-range potential and a frozen coating has enabled us to obtain quantitative agreement with experiment for DPPC SLBs in the fluid phase, at 323 K. For the DPPC gel phase, the matching is less satisfactory, but a wall represented by the potential $U_{\text{wall}}$ of P4 particles with a density $\rho^{\text{wall}} \simeq 9$ part·nm$^{-3}$ seems a reasonable initial choice to simulate both fluid and gel DPPC

SLBs, or SLBs with both fluid and gel domains.

# 4 Conclusions

This article reports molecular dynamics simulations of supported lipidic DPPC and DAPC neutral bilayers using the coarse-grained Martini model. To go beyond the previous work by Koutsioubas[13], we have enabled hydration variation and lipid flip/flop in the SLBs simulations and have investigated different substrate models. Our results emphasize the importance of including a long-range attraction to counterbalance the entropic repulsion between fluid membranes and the substrate. The parameters of the model, in particular the long-range potential representing the interaction with the wall, can be optimized so as to match the neutron specular reflectivity curves obtained from the simulations to those obtained experimentally.

For the future, one can further explore the possibilities of this flexible and generic model to match other experimental data, such as the adsorption energy. Our approach can also be easily adapted to model substrates with patterns, roughness or chemical complexity, which are becoming common in lipid-nanostructure hybrids, and are beyond the reach of all-atom molecular dynamics simulations.

# Acknowledgement

The authors thank GENCI (grant A0050807662) and the Pôle Scientifique de Modélisation Numérique (PSMN, Ecole Normale Supérieure de Lyon) for the allocation of High Performance Computing resources. A. Koutsiousbas is thanked for his kind sharing of experimental and simulation data, and for discussions. C. Domene and co-workers are thanked for their kind sharing of NeutronRefTool[12].

## Supporting Information Available

The file `supplementary_materials.pdf` is available free of charge and contains

- Details of the Simulation Protocol.
- Characterization of the Local Perturbation in the Bilayer due to the Pore.
- Ad-hoc analytical Model to fit the hydration layer thickness $\langle t_{\mathrm{W}}^{\mathrm{P}} \rangle$ in Fig. 8.
- Formalism and results of the calculations of Neutron Reflectometry Curves.

## References


(1) Sackmann, E. Supported Membranes: Scientific and Practical Applications. Science **1996**, 271, 43–48.

(2) Castellana, E. T.; Cremer, P. S. Solid supported lipid bilayers: From biophysical studies to sensor design. Surf. Sci. Rep. **2006**, 61, 429–444.

(3) Lee, Y. K.; Lee, H.; Nam, J.-M. Lipid-nanostructure hybrids and their applications in nanobiotechnology. NPG Asia Mater **2013**, 5, e48–e48.

(4) Jackman, J. A.; Cho, N. J. Supported Lipid Bilayer Formation: Beyond Vesicle Fusion. Langmuir **2020**, 36, 1387–1400.

(5) Katsaras, J.; Kučerka, N.; Nieh, M.-P. Structure from substrate supported lipid bilayers (Review). Biointerphases **2008**, 3, FB55–FB63.

(6) Charitat, T.; Bellet-Amalric, E.; Fragneto, G.; Graner, F. Adsorbed and free lipid bilayers at the solid-liquid interface. European Physical Journal B **1999**, 8, 583–593.

(7) Fragneto, G.; Charitat, T.; Daillant, J. Floating lipid bilayers: Models for physics and biology. Eur Biophys J **2012**, 41, 863–874.

(8) Motegi, T.; Yamazaki, K.; Ogino, T.; Tero, R. Substrate-Induced Structure and Molecular Dynamics in a Lipid Bilayer Membrane. Langmuir **2017**, 33, 14748 – 14755.

(9) Lee, T. H.; Hirst, D. J.; Kulkarni, K.; Del Borgo, M. P.; Aguilar, M. I. Exploring Molecular-Biomembrane Interactions with Surface Plasmon Resonance and Dual Polarization Interferometry Technology: Expanding the Spotlight onto Biomembrane Structure. Chemical Reviews **2018**, 118, 5392–5487.

(10) Okur, H. I.; Tarun, O. B.; Roke, S. Chemistry of Lipid Membranes from Models to Living Systems: A Perspective of Hydration, Surface Potential, Curvature, Confinement and Heterogeneity. J. Am. Chem. Soc. **2019**, 141, 12168–12181.

(11) Heinrich, F.; Lösche, M. Zooming in on disordered systems: Neutron reflection studies of proteins associated with fluid membranes. Biochimica et Biophysica Acta (BBA) - Biomembranes **2014**, 1838, 2341–2349.

(12) Darré, L.; Iglesias-Fernandez, J.; Kohlmeyer, A.; Wacklin, H.; Domene, C. Molecular Dynamics Simulations and Neutron Reflectivity as an Effective Approach To Characterize Biological Membranes and Related Macromolecular Assemblies. J. Chem. Theory Comput. **2015**, 11, 4875–4884.

(13) Koutsioubas, A. Combined Coarse-Grained Molecular Dynamics and Neutron Reflectivity Characterization of Supported Lipid Membranes. J. Phys. Chem. B **2016**, 120, 11474–11483.

(14) Willems, N.; Urtizberea, A.; Verre, A. F.; Iliut, M.; Lelimousin, M.; Hirtz, M.; Vijayaraghavan, A.; Sansom, M. S. Biomimetic Phospholipid Membrane Organization on Graphene and Graphene Oxide Surfaces: A Molecular Dynamics Simulation Study. ACS Nano **2017**, 11, 1613–1625.

(15) Lolicato, F.; Joly, L.; Martinez-Seara, H.; Fragneto, G.; Scoppola, E.; Baldelli Bombelli, F.; Vattulainen, I.; Akola, J.; Maccarini, M. The Role of Temper-

ature and Lipid Charge on Intake/Uptake of Cationic Gold Nanoparticles into Lipid Bilayers. Small **2019**, 15, 1805046.

(16) Xing, C.; Ollila, O. S.; Vattulainen, I.; Faller, R. Asymmetric nature of lateral pressure profiles in supported lipid membranes and its implications for membrane protein functions. Soft Matter **2009**, 5, 3258.

(17) Fuhrmans, M.; Müller, M. Mechanisms of Vesicle Spreading on Surfaces: Coarse-grained Simulations. Langmuir **2013**, 29, 4335–4349.

(18) Kong, X.; Lu, D.; Wu, J.; Liu, Z. Spreading of a Unilamellar Liposome on Charged Substrates: A Coarse-Grained Molecular Simulation. Langmuir **2016**, 32, 3785–3793.

(19) Mhashal, A. R.; Roy, S. Self-assembly of phospholipids on flat supports. Phys. Chem. Chem. Phys. **2015**, 17, 31152–31160.

(20) Gurtovenko, A. A.; Mukhamadiarov, E. I.; Kostritskii, A. Y.; Karttunen, M. Phospholipid–Cellulose Interactions: Insight from Atomistic Computer Simulations for Understanding the Impact of Cellulose-Based Materials on Plasma Membranes. J. Phys. Chem. B **2018**, 122, 9973–9981.

(21) Hirtz, M.; Kumar, N.; Chi, L. Simulation Modeling of Supported Lipid Membranes – A Review. CTMC **2014**, 14, 617–623.

(22) Tero, R. Substrate Effects on the Formation Process, Structure and Physicochemical Properties of Supported Lipid Bilayers. Materials **2012**, 5, 2658–2680.

(23) Blachon, F.; Harb, F.; Munteanu, B.; Piednoir, A.; Fulcrand, R.; Charitat, T.; Fragneto, G.; Pierre-Louis, O.; Tinland, B.; Rieu, J.-P. Nanoroughness Strongly Impacts Lipid Mobility in Supported Membranes. Langmuir **2017**, 33, 2444–2453.

(24) Goodchild, J. A.; Walsh, D. L.; Connell, S. D. Nanoscale Substrate Roughness Hinders Domain Formation in Supported Lipid Bilayers. Langmuir **2019**, 35, 15352–15363.

(25) Liang, Q.; Ma, Y. Q. Inclusion-mediated lipid organization in supported membranes on a patterned substrate. Journal of Physical Chemistry B **2008**, 112, 1963–1967.

(26) de Jong, D.; Heuer, A. The influence of solid scaffolds on flat and curved lipid membranes. AIP Adv. **2017**, 7, 075007.

(27) Vishnyakov, A.; Li, T.; Neimark, A. V. Adhesion of Phospholipid Bilayers to Hydroxylated Silica: Existence of Nanometer-Thick Water Interlayers. Langmuir **2017**, 33, 13148–13156.

(28) Marrink, S. J.; de Vries, A. H.; Mark, A. E. Coarse Grained Model for Semiquantitative Lipid Simulations. J. Phys. Chem. B **2004**, 108, 750–760.

(29) Marrink, S. J.; Risselada, H. J.; Yefimov, S.; Tieleman, D. P.; de Vries, A. H. The MARTINI Force Field: Coarse Grained Model for Biomolecular Simulations. J. Phys. Chem. B **2007**, 111, 7812–7824.

(30) Perlmutter, J. D.; Sachs, J. N. Experimental verification of lipid bilayer structure through multi-scale modeling. Biochimica et Biophysica Acta - Biomembranes **2009**, 1788, 2284–2290.

(31) Marrink, S. J.; Tieleman, D. P. Perspective on the Martini model. Chem. Soc. Rev. **2013**, 42, 6801.

(32) Xing, C.; Faller, R. Interactions of Lipid Bilayers with Supports: A Coarse-Grained Molecular Simulation Study. J. Phys. Chem. B **2008**, 112, 7086–7094.

(33) Bennun, S. V.; Dickey, A. N.; Xing, C.; Faller, R. Simulations of biomembranes and water: Important technical aspects. Fluid Phase Equilib. **2007**, 261, 18–25.

(34) Yesylevskyy, S. O.; Schäfer, L. V.; Sengupta, D.; Marrink, S. J. Polarizable Water Model for the Coarse-Grained MARTINI Force Field. PLoS Comput Biol **2010**, 6, e1000810.

(35) Lamberg, A.; Taniguchi, T. Coarse-Grained Computational Studies of Supported Bilayers: Current Problems and Their Root Causes. J. Phys. Chem. B **2014**, 118, 10643–10652.

(36) I. Hoopes, M.; L. Longo, M.; Faller, R. Computational Modeling of Curvature Effects in Supported Lipid Bilayers. CNANO **2011**, 7, 716–720.

(37) Liu, C.; Faller, R. Conformational, Dynamical. and Tensional Study of Tethered Bilayer Lipid Membranes in Coarse-Grained Molecular Simulations. Langmuir **2012**, 28, 15907–15915.

(38) Lin, X.; Wang, C.; Wang, M.; Fang, K.; Gu, N. Computer Simulation of the Effects of Nanoparticles' Adsorption on the Properties of Supported Lipid Bilayer. J. Phys. Chem. C **2012**, 116, 17960–17968.

(39) Risselada, H. J.; Marrink, S. J. Curvature effects on lipid packing and dynamics in liposomes revealed by coarse grained molecular dynamics simulations. Phys. Chem. Chem. Phys. **2009**, 11, 2056.

(40) Abraham, M. J.; Murtola, T.; Schulz, R.; Páll, S.; Smith, J. C.; Hess, B.; Lindah, E. Gromacs: High performance molecular simulations through multi-level parallelism from laptops to supercomputers. SoftwareX **2015**, 1-2, 19–25.

(41) de Jong, D. H.; Baoukina, S.; Ingólfsson, H. I.; Marrink, S. J. Martini straight: Boosting performance using a shorter cutoff and GPUs. Comput. Phys. Commun. **2016**, 199, 1–7.

(42) Benedetti, F.; Loison, C. Comment to: "martini straight: Boosting performance using a shorter cutoff and GPUs" by D.H. de Jong, S. Baoukina, H.I. Ingólfsson, and S.J. Marrink. Comput. Phys. Commun. **2018**, 228, 146–151.

(43) Martínez, L.; Andrade, R.; Birgin, E.; Martínez, J. PACKMOL: A package for building

initial configurations for molecular dynamics simulations. J. Comput. Chem. **2009**, 30, 2157–2164.

(44) Humphrey, W.; Dalke, A.; Schulten, K. VMD: Visual molecular dynamics. J. Mol. Graphics **1996**, 14, 33–38.

(45) Buchoux, S. FATSLiM: A fast and robust software to analyze MD simulations of membranes. Bioinformatics **2016**, 33, 133–134.

(46) Benedetti, F. 2020; `https://github.com/fben94/fatslim`.

(47) Benedetti, F.; Loison, C. 2020; `https://github.com/fben94/GJB`.

(48) Dabkowska, A. P.; Collins, L. E.; Barlow, D. J.; Barker, R.; Mclain, S. E.; Lawrence, M. J.; Lorenz, C. D. Modulation of dipalmitoylphosphatidylcholine monolayers by dimethyl sulfoxide. Langmuir **2014**, 30, 8803–8811.

(49) Hughes, A. V.; Ciesielski, F.; Kalli, A. C.; Clifton, L. A.; Charlton, T. R.; Sansom, M. S.; Webster, J. R. On the interpretation of reflectivity data from lipid bilayers in terms of molecular-dynamics models. Acta Crystallographica Section D: Structural Biology **2016**, 72, 1227–1240.

(50) Richard J. Gowers,; Max Linke,; Jonathan Barnoud,; Tyler J. E. Reddy,; Manuel N. Melo,; Sean L. Seyler,; Jan Domański,; David L. Dotson,; Sébastien Buchoux,; Ian M. Kenney, et al. MDAnalysis: A Python Package for the Rapid Analysis of Molecular Dynamics Simulations. Proceedings of the 15th Python in Science Conference. 2016; pp 98 – 105.

(51) Michaud-Agrawal, N.; Denning, E. J.; Woolf, T. B.; Beckstein, O. MDAnalysis: A toolkit for the analysis of molecular dynamics simulations. J. Comput. Chem. **2011**, 32, 2319–2327.

(52) Ehlers, J.; Hepp, K.; Board, E.; Beig, R.; Domcke, W.; Frisch, U.; Hillebrandt, W.; Jaffe, R. L. In X-ray and Neutron Reflectivity; Daillant, J., Gibaud, A., Eds.; Lecture Notes in Physics; Springer Berlin Heidelberg: Berlin, Heidelberg, 2009; Vol. 770.

(53) Helfrich, W.; Servuss, R.-M. Undulations, steric interaction and cohesion of fluid membranes. Il Nuovo Cimento D **1984**, 3, 137–151.

(54) Manghi, M.; Destainville, N. Statistical Mechanics and Dynamics of Two Supported Stacked Lipid Bilayers. Langmuir **2010**, 26, 4057–4068.

(55) Gerelli, Y.; Porcar, L.; Fragneto, G. Lipid Rearrangement in DSPC/DMPC Bilayers: A Neutron Reflectometry Study. Langmuir **2012**, 28, 15922–15928.

(56) Miettinen, M. S.; Lipowsky, R. Bilayer Membranes with Frequent Flip-Flops Have Tensionless Leaflets. Nano Letters **2019**, 19, 5011–5016.

(57) Hossein, A.; Deserno, M. Spontaneous Curvature, Differential Stress, and Bending Modulus of Asymmetric Lipid Membranes. Biophysical Journal **2020**, 118, 624–642.

(58) Daillant, J.; Bellet-Amalric, E.; Braslau, A.; Charitat, T.; Fragneto, G.; Graner, F.; Mora, S.; Rieutord, F.; Stidder, B. Structure and fluctuations of a single floating lipid bilayer. The Proceding of the National Academy of Sciences USA **2005**, 102, 11639–11644.

(59) Khelashvili, G.; Kollmitzer, B.; Heftberger, P.; Pabst, G.; Harries, D. Calculating the bending modulus for multicomponent lipid membranes in different thermodynamic phases. Journal of Chemical Theory and Computation **2013**, 9, 3866–3871.

(60) Nagle, J. F. Experimentally determined tilt and bending moduli of single-component lipid bilayers. Chemistry and Physics of Lipids **2017**, 205, 18–24.

(61) Chaurasia, A. K.; Rukangu, A. M.; Philen, M. K.; Seidel, G. D.; Freeman, E. C. Evaluation of bending modulus of lipid bilayers using undulation and orientation analysis. Physical Review E **2018**, 97, 1–12.

(62) Hemmerle, A.; Malaquin, L.; Charitat, T.; Lecuyer, S.; Fragneto, G.; Daillant, J. Controlling interactions in supported bilayers from weak electrostatic repulsion to high osmotic pressure. Proceedings of the National Academy of Sciences **2012**, 109, 19938–19942.

(63) Mecke, K. R.; Charitat, T.; Graner, F. Fluctuating lipid bilayer in an arbitrary potential: Theory and experimental determination of bending rigidity. Langmuir **2003**, 19, 2080–2087.

(64) Lipowsky, R.; Leibler, S. Unbinding Transitions of Interacting Membranes. Physical Review Letters **1986**, 56, 2541.

(65) McCluskey, A. R.; Grant, J.; Smith, A. J.; Rawle, J. L.; Barlow, D. J.; Lawrence, M. J.; Parker, S. C.; Edler, K. J. Assessing molecular simulation for the analysis of lipid monolayer reflectometry. Journal of Physics Communications **2019**, 3.

(66) Bergström, L. Hamaker constants of inorganic materials. Advances in Colloid and Interface Science **1997**, 70, 125 – 169.

(67) Oleson, T. A.; Sahai, N. Interaction energies between oxide surfaces and multiple phosphatidylcholine bilayers from extended-DLVO theory. Journal of Colloid and Interface Science **2010**, 352, 316–326.

(68) Kowalik, B.; Schlaich, A.; Kanduč, M.; Schneck, E.; Netz, R. R. Hydration Repulsion Difference between Ordered and Disordered Membranes Due to Cancellation of Membrane–Membrane and Water-Mediated Interactions. J. Phys. Chem. Lett. **2017**, 8, 2869–2874.

# Graphical TOC Entry